NASA TM-80121

NASA Technical Memorandum 80121

NASA-TM-80121 19790019074

EXPERIMENTAL AND ANALYTICAL STUDY OF FATIGUE DAMAGE IN NOTCHED GRAPHITE/EPOXY LAMINATES

John D. Whitcomb

June 1979

National Aeronautics and
Space Administration

Langley Research Center
Hampton, Virginia 23665

EXPERIMENTAL AND ANALYTICAL STUDY OF FATIGUE DAMAGE IN NOTCHED GRAPHITE/EPOXY LAMINATES

John D. Whitcomb
NASA Langley Research Center
Hampton, Virginia 23665

ABSTRACT

Fatigue damage development in notched $(0/\pm45/0)_s$, $(45/0/-45/0)_s$, $(90/\pm45/0)_s$, and $(45/90/-45/0)_s$ graphite/epoxy laminates was investigated. Both tension and compression fatigue behaviors were studied. Most of the tests were conducted at load levels equal to two-thirds of the ultimate tensile strength of the notched specimens. After fatigue loading, specimens were examined for damage type and location using visual inspection, light microscopy, scanning electron microscopy, ultrasonic C-scans, and X-radiography. Delamination and ply cracking were found to be the dominant types of fatigue damage. In general, ply cracks did not propagate into adjacent plies of differing fiber orientation. To help understand the varied fatigue observations, the interlaminar stress distribution was calculated with finite element analysis for the regions around the hole and along the straight free edge. Comparison of observed delamination locations with the calculated stresses indicated that both interlaminar shear and peel stresses must be considered when predicting delamination. The effects of the fatigue cycling on residual strength and stiffness were measured for some specimens of each laminate type. Fatigue loading generally caused only small stiffness losses. In all cases, residual strengths were greater than or equal to the virgin strengths.

INTRODUCTION

Confidence in the long-term reliability of composite materials must precede full exploitation of their high specific strengths and stiffnesses. To gain this confidence the fatigue behavior needs to be understood. Understanding composite fatigue behavior is a formidable task because of the diverse kinds of fibers, matrix materials, fiber orientations, and stacking sequences, and the concomitant variety of fatigue damage processes. Fatigue data in the form of stress versus cycles to failure for one laminate are not generally applicable to other laminates with different stacking sequences and certainly not those with different fiber orientations. To avoid testing all conceivable laminates, a generic fatigue analysis that predicts the fatigue behavior for any laminate from limited basic fatigue data is desirable.

The first step toward developing a generic fatigue analysis is to understand the basic fatigue damage processes in specific composite laminates. Tests (e.g., refs. 1-4) and analyses (e.g., refs. 5-7) reveal much about fatigue damage morphology and stress distributions in composites. Broken fibers, disbonded fibers, transthickness cracks, and intralaminar cracks have been shown to be primary forms of fatigue damage in boron/epoxy (ref. 1). For graphite/epoxy laminates, Foye (ref. 8) has shown that delamination is an important mode of damage propagation. Interlaminar stresses at straight free edges have been shown to be responsible for the initiation of delamination in graphite/epoxy laminates.

The objective of this paper is to systematically examine fatigue damage in several notched graphite/epoxy laminates and to compare the damage with stress distributions. First, specimens subjected to fatigue loading were examined for damage type and location with ultrasonic C-scans, visual inspection, X-radiography, scanning electron microscopy (SEM), and light microscopy (of specimen sections). Next, stress distributions were calculated using 3-D finite element analysis and were compared with the distribution of delaminations. Finally, the effects of the fatigue cycling on residual strength and stiffness were measured for some of the specimens of each laminate type.

SYMBOLS LIST

E_x, E_y, E_z	extensional moduli
e_o	specified axial strain
G_{xy}, G_{xz}, G_{yz}	shear moduli
R	ratio of minimum to maximum stress in fatigue cycle
S_{max}	peak fatigue stress
S_{ult}	ultimate tensile strength
S_x	gross axial stress
U, V, W	functions used to describe u, v, and w
u, v, w	displacements in x, y, and z directions, respectively
x, y, z	Cartesian coordinates
θ	polar coordinate
$\nu_{xy}, \nu_{xz}, \nu_{yz}$	Poisson ratios
σ_z	normal stress in z direction
τ_{xz}	shear stress in Cartesian coordinate system
$\tau_{\theta z}$	shear stress in cylindrical coordinate system

EXPERIMENTAL PROCEDURE AND APPARATUS

Specimens and Loading

The notched specimen configuration is shown in figure 1. Ultrasonically drilled holes in the specimens respresented structural discontinuities which cause stress concentration. Four laminates were considered. Two were orthotropic: $(0/\pm45/0)_s$ and $(45/0/-45/0)_s$. The other two were quasi-isotropic: $(90/\pm45/0)_s$ and $(45/90/-45/0)_s$. The specimens were made from T300/5209 tape. Average laminate thickness was about 0.96 mm; fiber volume was 67 percent.

The specimens were fatigue tested on servo-controlled hydraulic test machines under constant-amplitude, load-controlled, sinusoidal axial loading at a frequency of 10 Hz. For each stacking sequence of the two types of laminates, several specimens were tested with tension-tension ($R = 0.05$) loading. Several others were tested with compression-compression ($R = 20$) loading; guide plates (fig. 2) prevented buckling during compression loading. The maximum absolute gross-section stress applied during cyclic loading was 254 MPa for the orthotropic laminates and 195 MPa for the quasi-isotropic laminates. These stresses, which were approximately two-thirds of the ultimate tensile strength of the notched specimens, initially produced nominal absolute axial strains of 0.0033 and 0.0038 for the orthotropic and quasi-isotropic laminates, respectively. A few tensile fatigue tests were conducted at maximum cyclic stresses of approximately 80 percent of the static ultimate tensile strength. All measurements were taken in U.S. Customary Units.

Monitoring Fatigue Damage

Various techniques were used to locate damage. Ultrasonic C-scan records were used to locate delaminations over the length and width of the specimen. Some specimens were then sectioned with a low-speed diamond circular saw. Cutting-induced damage was minimized by sandwiching the graphite-epoxy between aluminum sheets. The sections were then polished for examination by light microscopy. These section studies were useful both for locating the particular ply interface at which delamination occurred and to locate damage, such as ply cracking, not detected by the C-scan. Radiographs, enhanced with tetrabromoethane, were used to determine the direction of ply-crack propagation. A scanning electron microscope (SEM) was used to examine the fracture surfaces of the specimens tested for residual strength. The SEM was used to detect fiber disbonding, as evidenced by fiber pullout. Visual inspection was used to determine surface crazing. Also, the matrix in a few unbroken fatigue specimens was burned away (ref. 9) to separate the plies for individual examination for fiber breakage; this procedure is referred to as deplying.

The effects of fatigue damage on stiffness and strength were measured. Gross stiffness was calculated from elongation measurements made over a 100-mm gage length with a linear variable differential transformer (fig. 2). Residual tensile strengths were measured after 10^7 tensile or compressive load cycles.

STRESS ANALYSIS

To help understand the fatigue behavior, the interlaminar stress distribution was calculated, with finite element analysis, for the regions around the hole and along the straight edge. Only the effects of mechanical loading were considered. Thermal residual stresses and moisture-induced stresses were not considered. A conventional 3-D finite element analysis was used to analyze the region near the hole, and a 3-D analysis, modified to impose uniform axial strain (ref. 5), was used to analyze the region near the straight edge. Both analyses were displacement formulations.

A schematic of an unnotched specimen analyzed for stresses at the straight free edge is shown in figure 3(a). The requirement for uniform axial strain may be stated as follows:

$$u = e_o x + U(y,z)$$

$$v = V(y,z)$$

$$w = W(y,z)$$

where u, v, and w are the displacements in the x, y, and z directions, respectively. In the analysis, e_o is the specified axial strain. Because the three unknowns U, V, and W are functions of only y and z, the cross section of the specimen can be modeled by two-dimensional elements with 3 degrees of freedom per node. Symmetry conditions permit solution of the problem by analysis of only one-fourth of the cross section. The finite element model used in the edge analysis is shown in figure 3(b). Eight-node isoparametric quadrilateral elements were used. Boundary conditions were,

$$\text{at } y = 0: \; u = 0, \; v = 0,$$

$$\text{at } z = 0: \; w = 0.$$

The region around the hole was analyzed with a conventional 3-D finite element analysis. The analysis used a 20-node isoparametric element. Exploiting the polar and midplane symmetries (ref. 10), only one-fourth of the specimen was modeled, as shown in figure 3(c). The total number of degrees of freedom in the model was 3198. Unit axial displacements were specified at $x = \pm 38$ mm. Other boundary conditions were:

$$\begin{aligned} \text{at}\quad y = 0 \qquad & u(x,0,z) = -u(-x,0,z) \\ & v(x,0,z) = -v(-x,0,z) \\ & w(x,0,z) = w(-x,0,z) \\ \text{at}\quad z = 0 \qquad & w(x,y,0) = 0 \end{aligned}$$

Material properties for a 0-deg ply were taken as follows (ref. 5):

$$E_x = 140 \text{ GPa}$$

$$E_y = E_z = 14 \text{ GPa}$$

$$G_{xy} = G_{xz} = G_{yz} = 5.9 \text{ GPA}$$

$$\nu_{xy} = \nu_{xz} = \nu_{yz} = 0.21$$

Properties for angle plies were obtained by appropriate coordinate transformations.

RESULTS AND DISCUSSION

First, the types of fatigue damage observed are discussed. Next, the initiation sites and propagation paths of fatigue damage are described. Then delamination locations are compared with the calculated interlaminar stress distributions. Finally, the effects of the fatigue damage on strength and stiffness are discussed.

Damage Type

The specimens were examined for delaminations, ply cracks, fiber disbonds, and fiber breaks. Typical delaminations and ply cracks are shown in figure 4. Radiographs of the specimens revealed that the ply cracks grew parallel to the fibers.

A few specimens that had been fatigue loaded at up to 80 percent of the notched tensile strength were deplied. Figure 5 shows a micrograph of a deplied lamina. Very few broken fibers were found. Apparently, fiber breakage was not a significant fatigue degradation mode for the laminates examined. In contrast, progressive fiber breakage has been observed in boron/epoxy laminates (ref. 1).

Fracture surfaces showed that fibers pulled out only a very short distance (fig. 6). The fiber pullout is indicative of fiber disbonding. However, fiber pullout was about the same for specimens with and without fatigue cycling, suggesting that the fatigue loading caused little fiber disbonding.

The various observations revealed that delamination and ply cracking were the primary mechanisms of fatigue degradation.

Location of Fatigue Damage

Generally, the plies cracked in the same region as they delaminated, but THE density of ply cracks did not correlate with the extent of the delaminations. The 0-deg plies cracked axially along tangents to the hole in all of the laminates. However, as shown in figure 7(a), axial cracks were sometimes confined to the 0-deg plies. Sometimes the axial cracks grew through the entire laminate thickness by linking of ply cracks with delaminations. In general, ply cracks did not propagate into adjacent plies of differing fiber orientation. In contrast, axial cracks in boron/epoxy specimens grow relatively straight through the thickness without linking by delaminations, as shown in figure 7(b).

The difference between the behaviors of the graphite/epoxy and boron/epoxy specimens may be a result of the different ply interface characteristics. The ply interfaces are more distinct and thinner in graphite/epoxy than in boron/epoxy. The thinner interface in graphite/epoxy is expected to create higher interlaminar stresses than in boron/epoxy. Cracks are deterred from propagating straight through the thickness from one ply to the next by delaminations. The remainder of this section will concentrate on the location of delaminations.

Figure 8 shows typical delamination locations for the specimen after 10^7 tension or compression fatigue loads. Comparison of figures 8(a) and 8(b) reveals that stacking sequence affected delamination growth. The $(0/\pm45/0)_s$ specimen delaminated above and below the hole, but the $(45/0/-45/0)_s$ specimen delaminated uniformly around the hole. The sign of the loading also affected delamination growth. For example, the $(45/0/-45/0)_s$ specimen delaminated much more extensively under compression (fig. 8(d)) than tension (fig. 8(b)). Fiber orientation also affected delamination growth; delamination growth from the hole was more closely alined with the load direction for the orthotropic specimens than for the quasi-isotropic specimens.

The delamination locations compare well with the stress distributions determined by a finite element stress analysis. Delaminations were more likely in areas where both the interlaminar shear and tensile peel stresses were high. However, some delaminations were found in areas of high interlaminar shear but where the analysis indicated the peel stresses were compressive. Figures 9, 10, and 11 show typical results.

Figure 9 shows the stress distribution at the straight edge of a $(90/\pm45/0)_s$ specimen. The stresses are normalized with respect to the gross axial laminate stress. The highest interlaminar stresses occurred between the +45-deg and -45-deg plies. The peel stress, σ_z, at this interface was compressive for tensile loading. Thus, based on the sign of σ_z, delamination should be more likely under compression than tension loading. Note that the C-scans shown in figures 8(a) and 8(c) corroborate this prediction; under tension fatigue straight-edge delamination did not occur, whereas under compression fatigue straight-edge delamination did occur. In other tests under higher tensile loads, edge delaminations occurred due to the high shear stresses in spite of the compressive normal stress.

Calculated interlaminar stresses and observed delamination for a notched $(90/\pm45/0)_s$ fatigue specimen are shown in figure 10. The schematic in figure 10(a) indicates the locations where the specimen was sectioned and examined and stresses were calculated. The stresses shown are those calculated at the edge of the hole. In this case, the stresses are normalized with respect to the absolute value of the gross axial stress. At 90 degrees the delaminations were associated with coincidental peaks in the shear and peel stresses between the 45-deg plies. At 120 degrees the shear ($\tau_{\theta z}$) stress peaks between the 0-deg and 45-deg plies caused delamination. At 160 degrees the tensile peel stress between the 0-deg plies appears to have governed the location of delamination.

Figure 11 shows results for a notched $(45/90/-45/0)_s$ fatigue specimen. At 90 degrees the delamination was associated with a small tensile peel stress and high shear stress. At 120 degrees the delamination was driven by high shear stresses, as it was in the $(90/\pm45/0)_s$ specimen at the same relative location. At about 175 degrees no delamination occurred at the edge of the hole. The delamination away from the edge was associated with shear-out of the 0-deg plies.

Delamination away from the edge of the hole cannot be predicted by an analysis based on an undamaged specimen because, after fatigue damage develops, stress distributions change. The change in stress distribution around the hole can even alter the direction of damage propagation, as shown in figure 12. For most of the test, the damage propagated at about 60 degrees to the load direction. Later in the test, damage propagated axially. These results point out the need for a stress analysis capable of calculating stresses after fatigue damage occurs.

Residual Stiffness and Tensile Strength

Stiffness was monitored during the fatigue tests and residual strength was determined for some of the specimens after fatigue loading.

Results of the stiffness measurements are presented in table I. The stiffness changes were generally quite small. Since the fatigue damage was restricted to the vicinity of the hole and the straight free edges, the lack of large changes was not surprising.

The strength measurements are shown in figure 13 and table II. In all cases the residual strength after 10^7 cycles was greater than or equal to the virgin strength. The increase in strength with fatigue probably is due to stress redistribution which accompanies fatigue damage. Interestingly, the fatigue damage responsible for the stress redistribution may not become part of the fracture surface. For example, during tension fatigue of a $(0/\pm45/0)_s$ specimen, delaminations grew predominantly axially above and below the hole (see fig. 8(a)). However, as shown in figure 14, the fracture was transverse.

CONCLUDING REMARKS

The fatigue behavior of four notched graphite/epoxy laminates was studied. Two of the laminates were orthotropic: $(0/\pm45/0)_s$ and $(45/0/-45/0)_s$. The other two were quasi-isotropic: $(90/\pm45/0)_s$ and $(45/90/-45/0)_s$. The specimens were tested at relatively high constant-amplitude tensile or compressive loads. Specimens were examined for fatigue damage type and location using ultrasonic C-scans, visual inspection, X-radiography, scanning electron microscopy, and light microscopy.

Fatigue damage was primarily delamination and ply cracking parallel to the fibers. In general, ply cracks did not propagate into adjacent plies of differing fiber orientation. In all cases the fatigue cycling of notched specimens resulted in residual strengths greater than or equal to the virgin strengths. Fatigue loading generally caused only small stiffness changes.

The location of delamination was sensitive to the fiber orientations, stacking sequence, and sign of the loading. Finite element stress analysis indicated that both interlaminar normal stress and shear stress must be considered to explain the observed delamination. Furthermore, the altered stress distribution, concomitant with fatigue damage growth, can change the direction of delamination propagation.

ACKNOWLEDGEMENTS

The laboratory work was performed by Mr. Joe C. Woolsey, a Langley Research Center engineering technician.

The computer codes used in this study were developed by Dr. I. S. Raju, a post-doctoral research fellow of the Joint Institute for Advancement of Flight Sciences, George Washington University, at Langley Research Center.

Specimens were deplied by Mr. Samuel Freeman of Lockheed-Georgia Company.

REFERENCES

1. Roderick, G. L.; and Whitcomb, J. D.: Fatigue Damage of Notched Boron/Epoxy Laminates Under Constant-Amplitude Loading. ASTM STP-636, 1977, pp. 73-88.

2. Daniel, I. M.; Rowlands, R. E.; and Whiteside, J. B.: Effects of Material and Stacking Sequence on Behavior of Composite Plates With Holes. J. Experimental Mechanics, January 1974, pp. 1-9.

3. Ramani, S. V.; and Williams, D. P.: Notched and Unnotched Fatigue Behavior of Angle-Ply Graphite/Epoxy Composites. ASTM STP-636, 1977, pp. 27-46.

4. Sturgeon, J. B.: Fatigue of Multi-Directional Carbon Fibre-Reinforced Plastics. J. Composites, October 1977, pp. 221-226.

5. Wang, A. S. D.; and Crossman, Frank W.: Some New Results on Edge Effect in Symmetric Composite Laminates. J. Composite Materials, vol. 11, January 1977, pp. 92-106.

6. Rybicki, E. F.; and Schmuesser, D. W.: Three-Dimensional Finite Element Stress Analysis of Laminated Plates Containing a Circular Hole. AFML-TR-76-92, 1976.

7. Ramkumar, R. L.; Kulkarni, S. V.; and Pipes, R. B.: Evaluation and Expansion of an Analytical Model for Fatigue of Notched Composite Laminates. NASA CR-145308, 1978.

8. Foye, R. L.; and Baker, D. J.: Design of Orthotropic Laminates. Presented at the AIAA/ASME 11th Conference on Structures, Structural Dynamics, and Materials, Denver, CO, April 1970.

9. Bailey, C. D.; Freeman, S. M.; and Hamilton, J. M.: Detection and Evaluation of Impact Damage in Graphite/Epoxy Composites. Proceedings of the Ninth National Technical Conference of the Society for the Advancement of Material and Process Engineering (Materials and Processes - In-Service Performance), Atlanta, GA, October 1977.

10. Raju, I. S.; and Crews, J. H., Jr.: Polar Symmetry in Three-Dimensional Analysis of Laminates With Angle Plies. (Formal citation should be available before publication of ASTM STP.)

11. Stinchcomb, W. W.; and Reifsnider, K. L.: Fatigue Damage Mechanisms in Composite Materials: A Review. Proceedings of ASTM Symposium on Fatigue Mechanisms, Kansas City, MO, May 1978.

TABLE I.- EFFECT OF FATIGUE CYCLING ON STIFFNESS

Laminate	Specimen number	Loading[a]	Change in stiffness
$(0/\pm45/0)_s$	2A6	T	0
	2A7	T	0
	2A13	T	0
	2A15	T	+5%
	2A16	C	-7%
	2A19	C	-3%
$(45/0/-45/0)_s$	1A6	T	0
	1A20	T	+5%
	1A13	C	-7%
	1A14	C	-7%
$(90/\pm45/0)_s$	3A6	T	0
	3A8	T	0
	3A14	T	+4%
	3A21	T	-6%
	3A24	T	-4%
	3A7	C	0
	3A19	C	0
	3A20	C	-4%
$(45/90/-45/0)_s$	4A6	T	0
	4A13	T	0
	4A14	T	+4%
	4A17	T	0
	4A1	C	-5%
	4A8	C	0
	4A20	C	-10%

[a] 10^7 cycles at $|S|_{max}/S_{ult} = 67\%$;
T ≡ tension, C ≡ compression

TABLE II.- STATIC TENSILE STRENGTHS OF NOTCHED SPECIMENS

Laminate	Specimen number	Preconditioning[a]	Gross failure stress, MPa
$(0/\pm45/0)_s$	2A3	None	389
	2A4	None	370
	2A5	None	370
	2A7	T	469
	2A13	T	489
	2A19	C	450
$(45/0/-45/0)_s$	1A3	None	402
	1A4	None	387
	1A5	None	373
	1A7	T	408
	1A20	T	486
	1A13	C	467
$(90/\pm45/0)_s$	3A3	None	282
	3A4	None	301
	3A5	None	299
	3A8	T	339
	3A14	T	301
	3A19	C	312
$(45/90/-45/0)_s$	4A3	None	292
	4A4	None	292
	4A5	None	282
	4A13	T	327
	4A14	T	342
	4A1	C	308

[a] None ≡ No fatigue cycles
T, C ≡ Tension, compression fatigue respectively at $|S|_{max}/S_{ult} = 67\%$ for 10^7 cycles

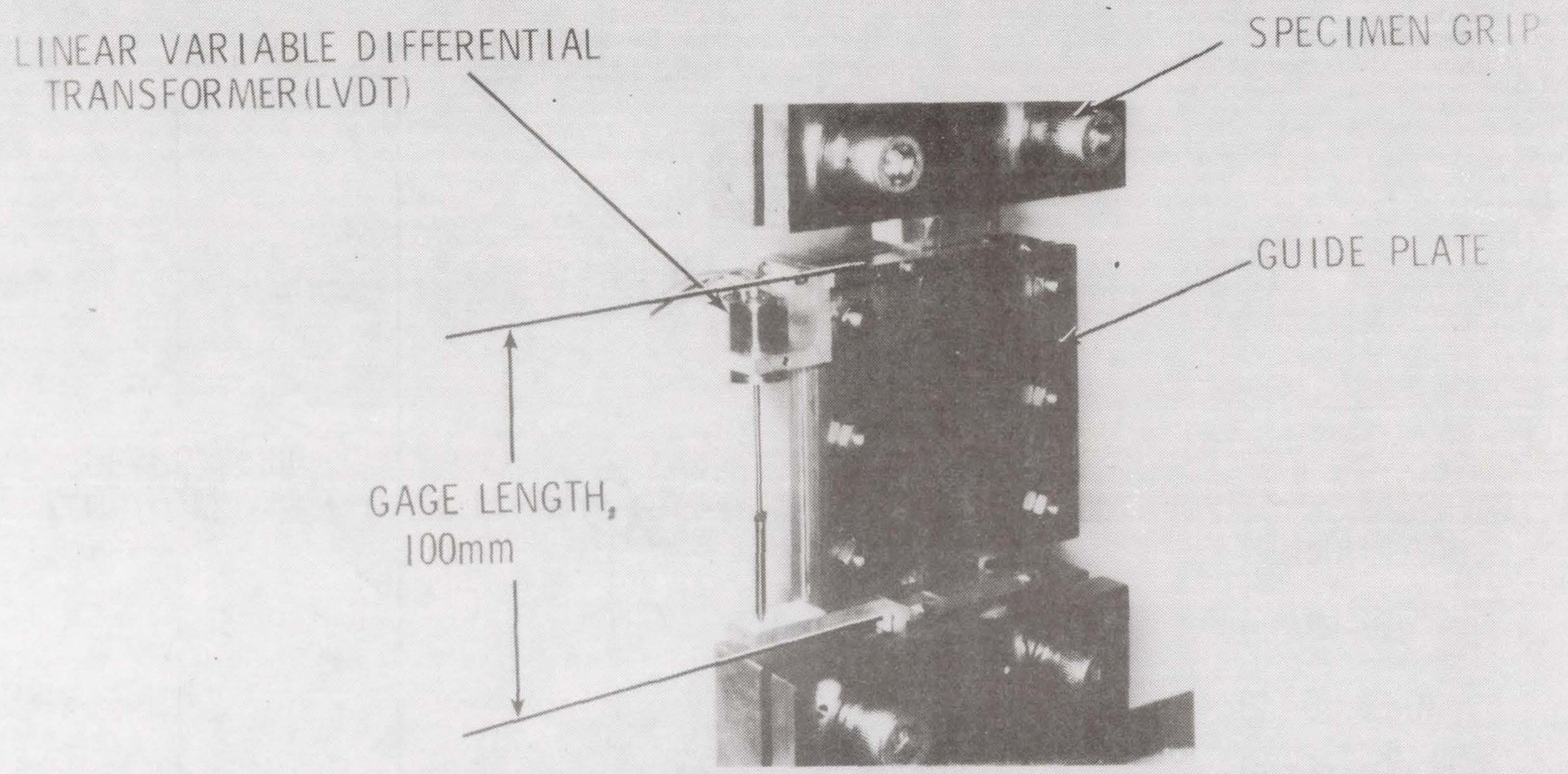

Figure 2.- Apparatus for stiffness measurement in tension and compression and lateral guide plates for compression tests.

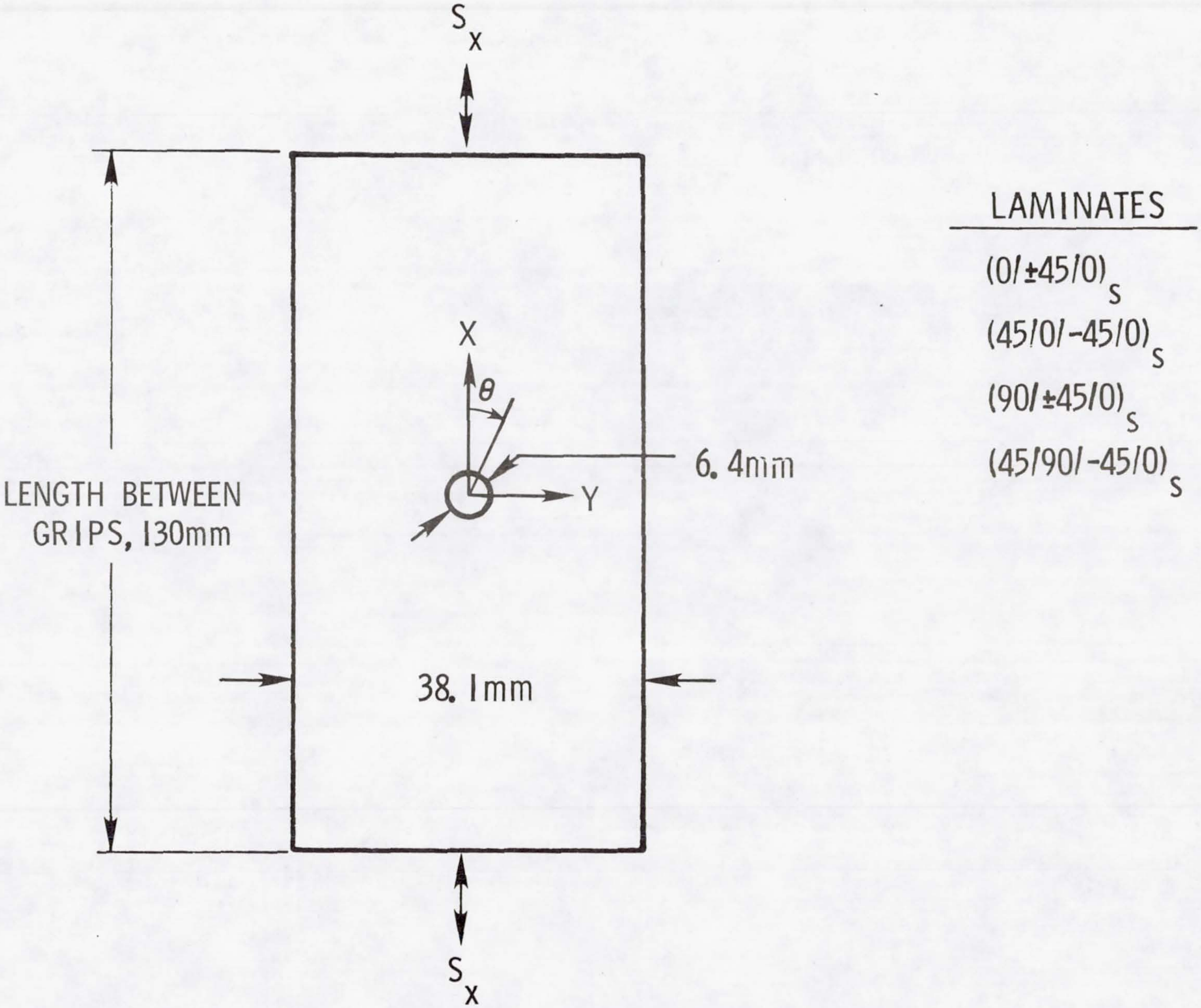

Figure 1.- Specimen configuration.

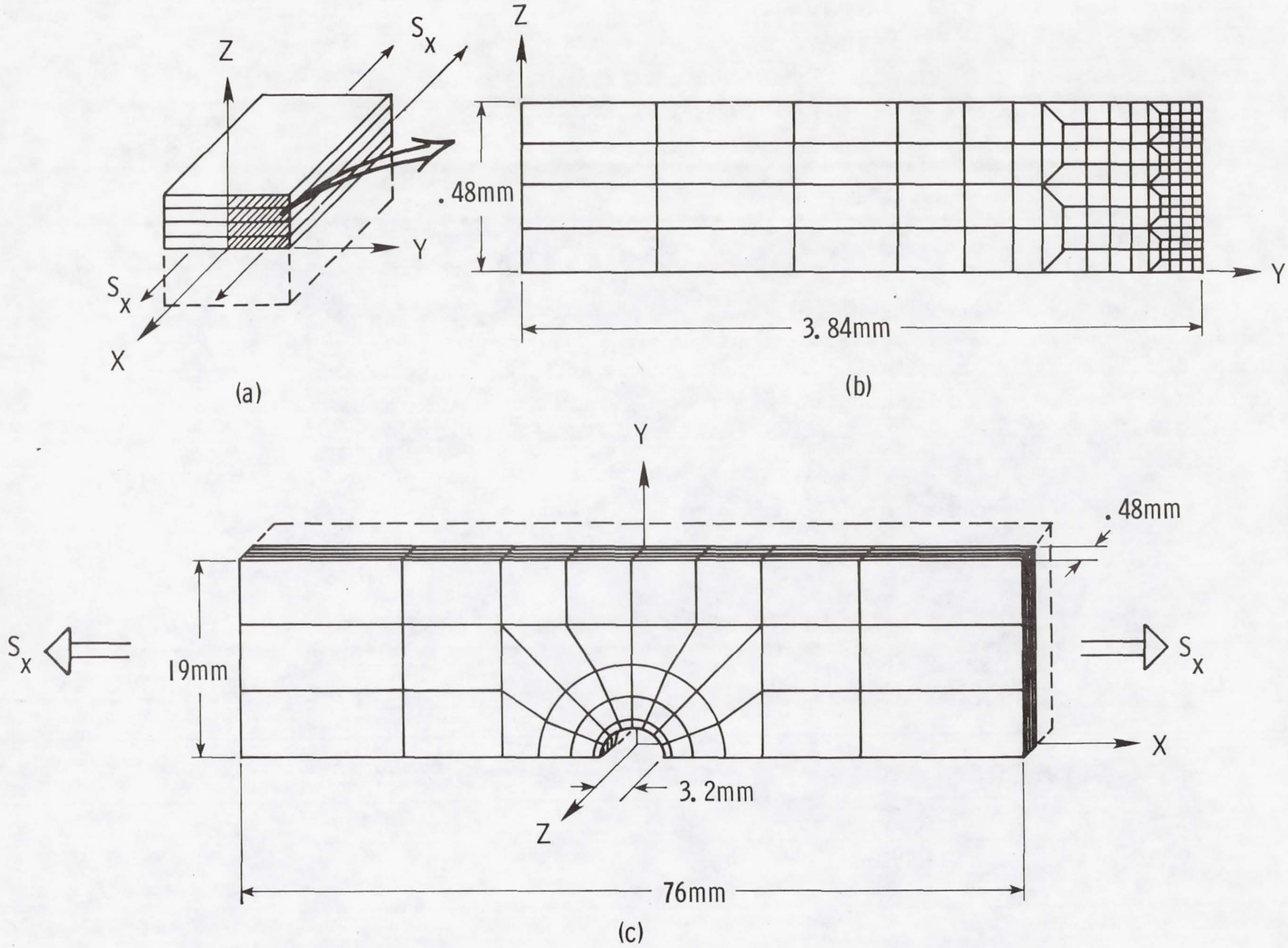

Figure 3.- Finite element models of straight edge and notch vicinity.

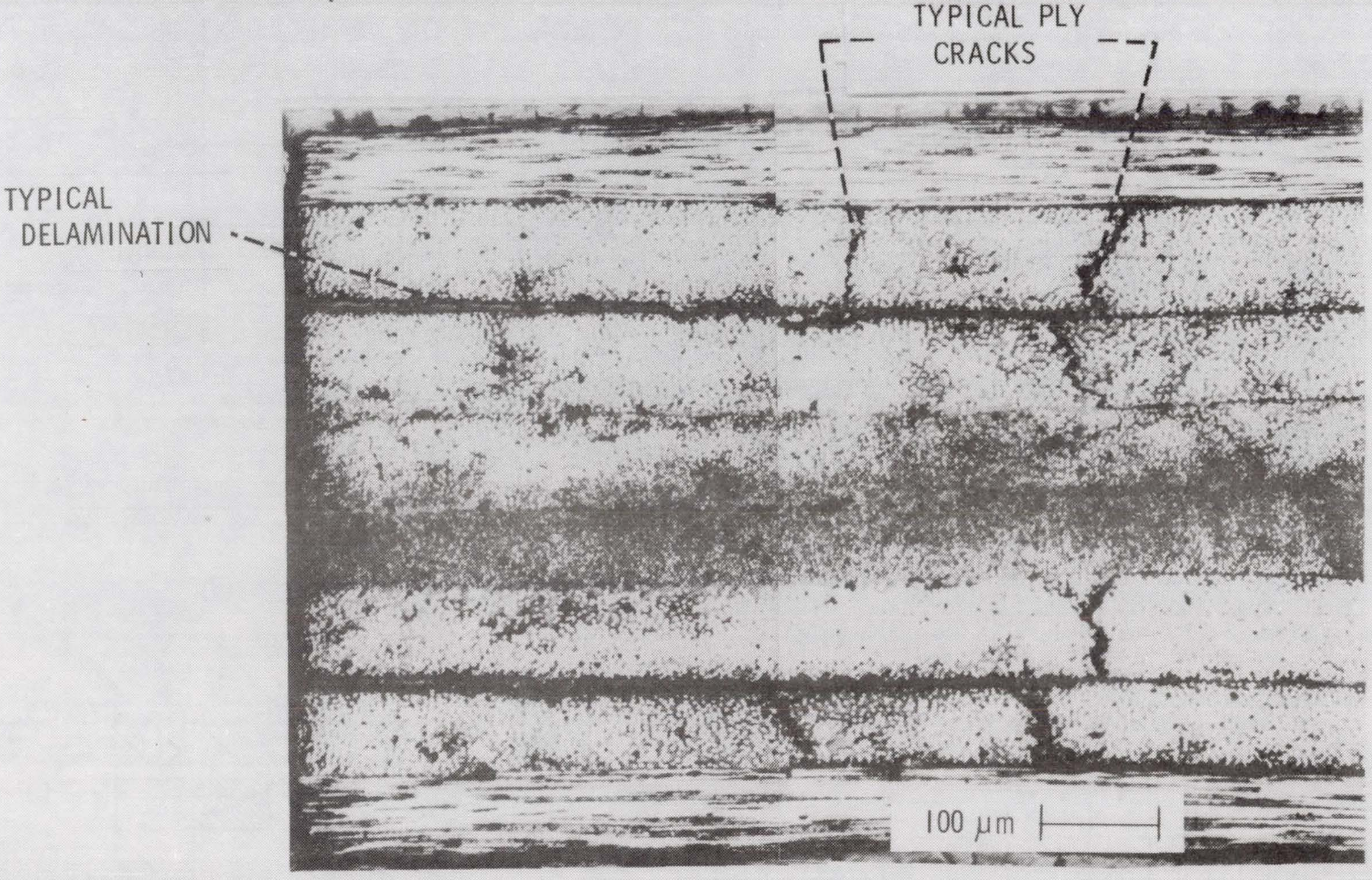

Figure 4.- Transverse section showing typical delaminations and ply cracks ($(90/\pm45/0)_s$ laminate).

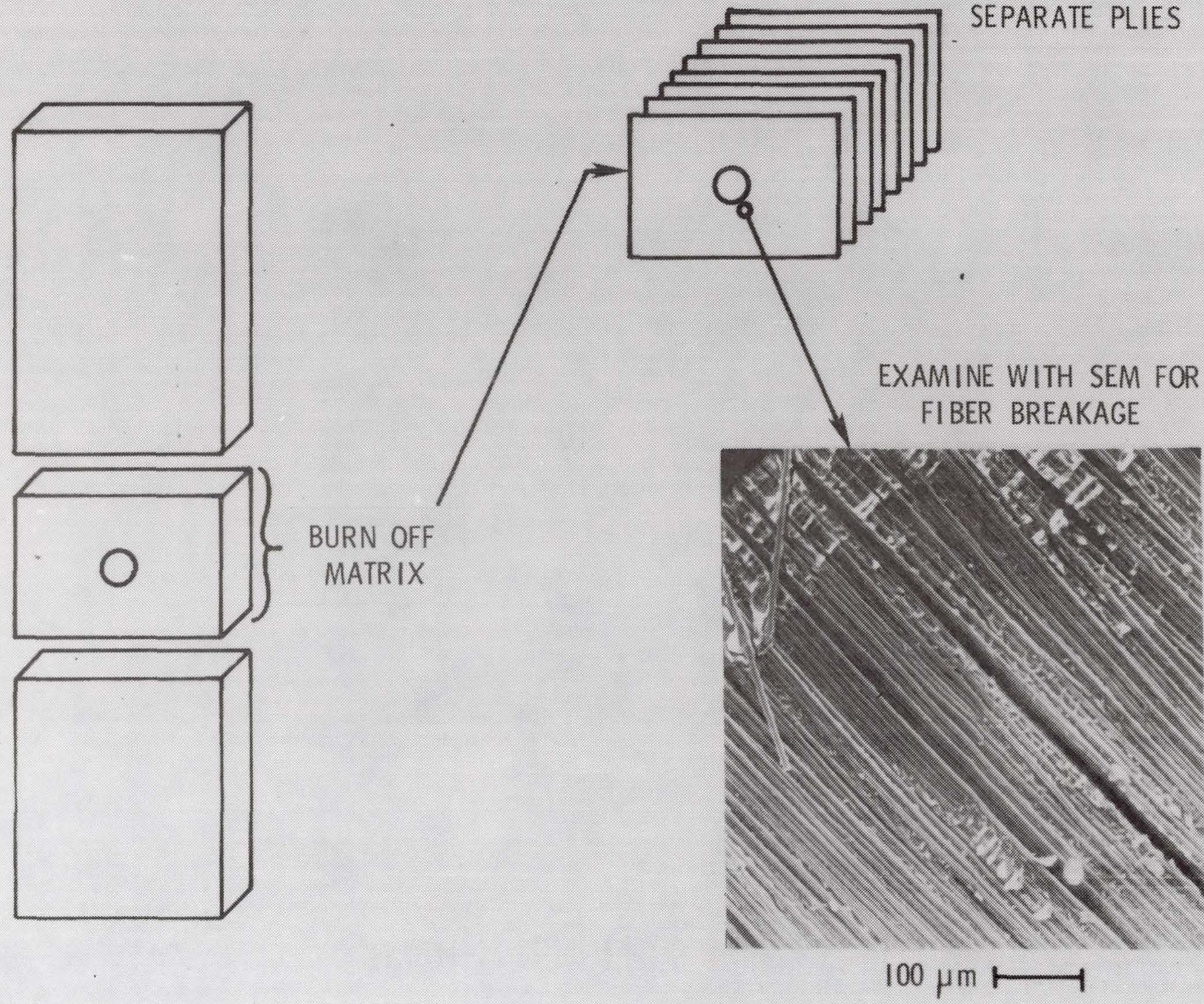

Figure 5.- Deply procedure.

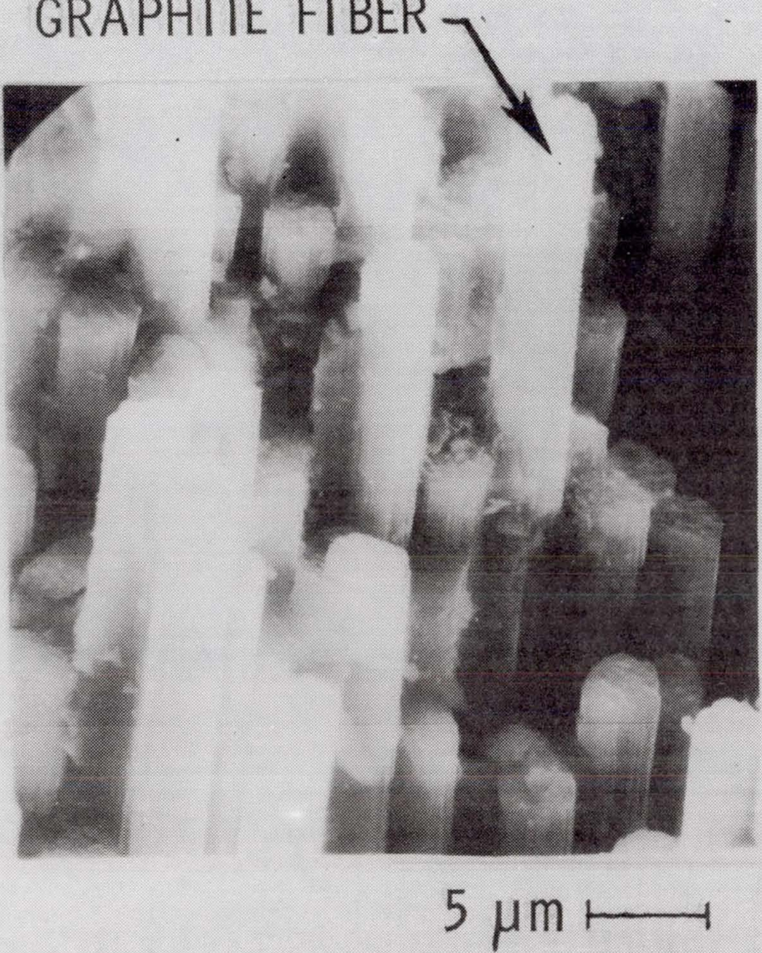

Figure 6.- Fracture surface of G/E fatigue specimen showing fiber pullout.

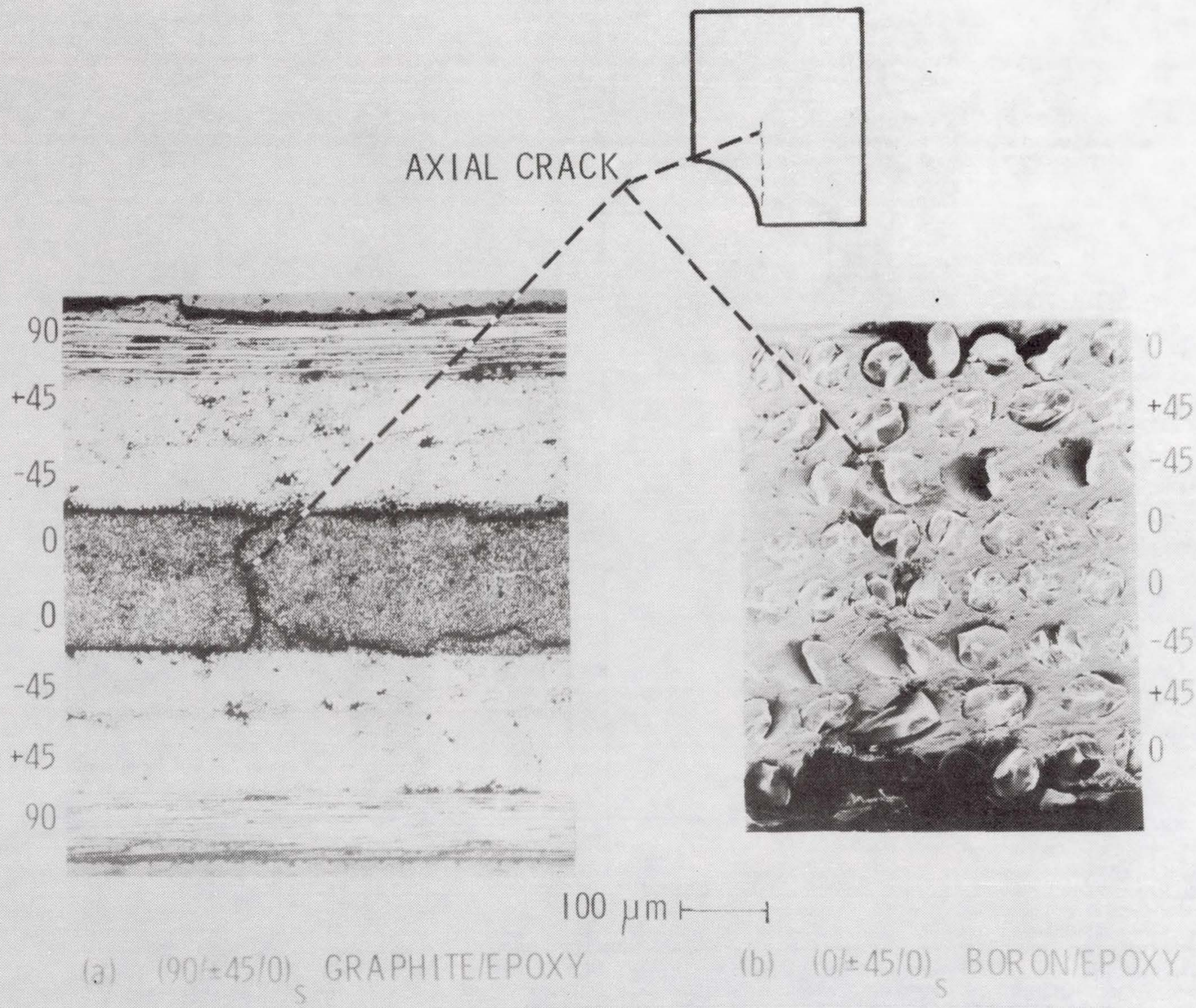

Figure 7.- Transverse sections of fatigue damaged laminates.

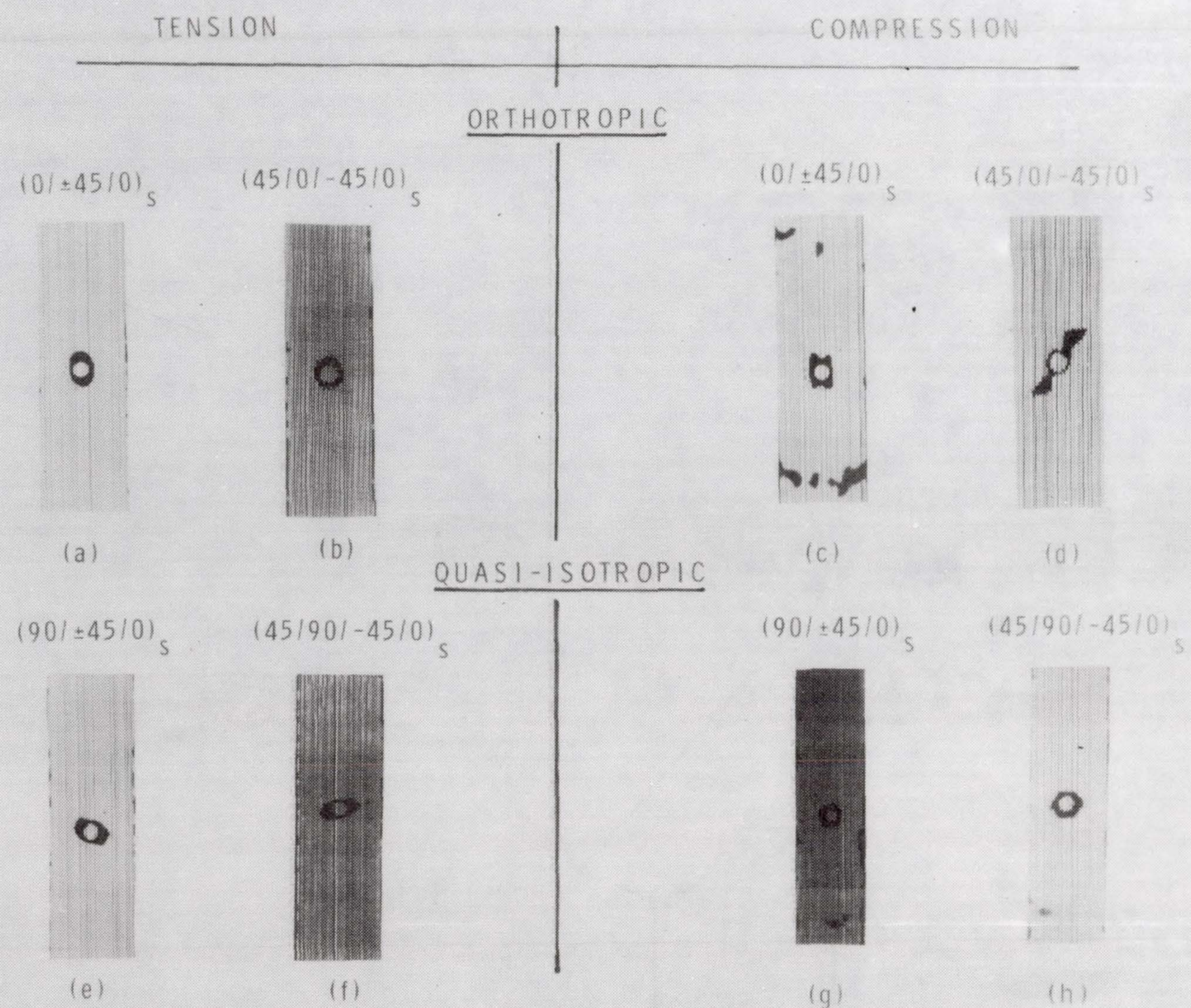

Figure 8.- C-scan records of various notched laminates after 10^7 tensile or compressive fatigue cycles.

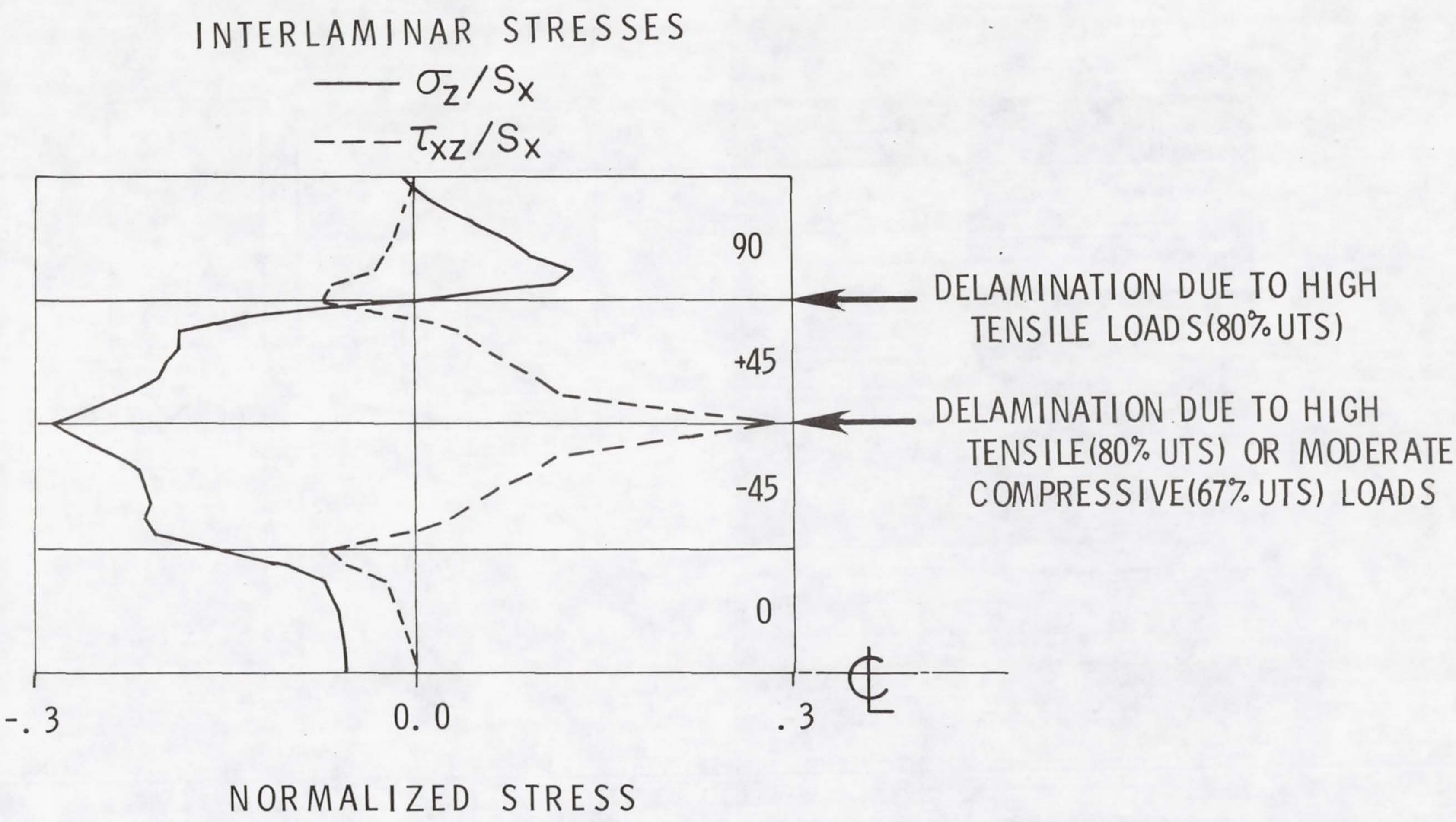

Figure 9.- Interlaminar stress distribution at straight edge and delamination locations for $(90/\pm45/0)_s$ laminate.

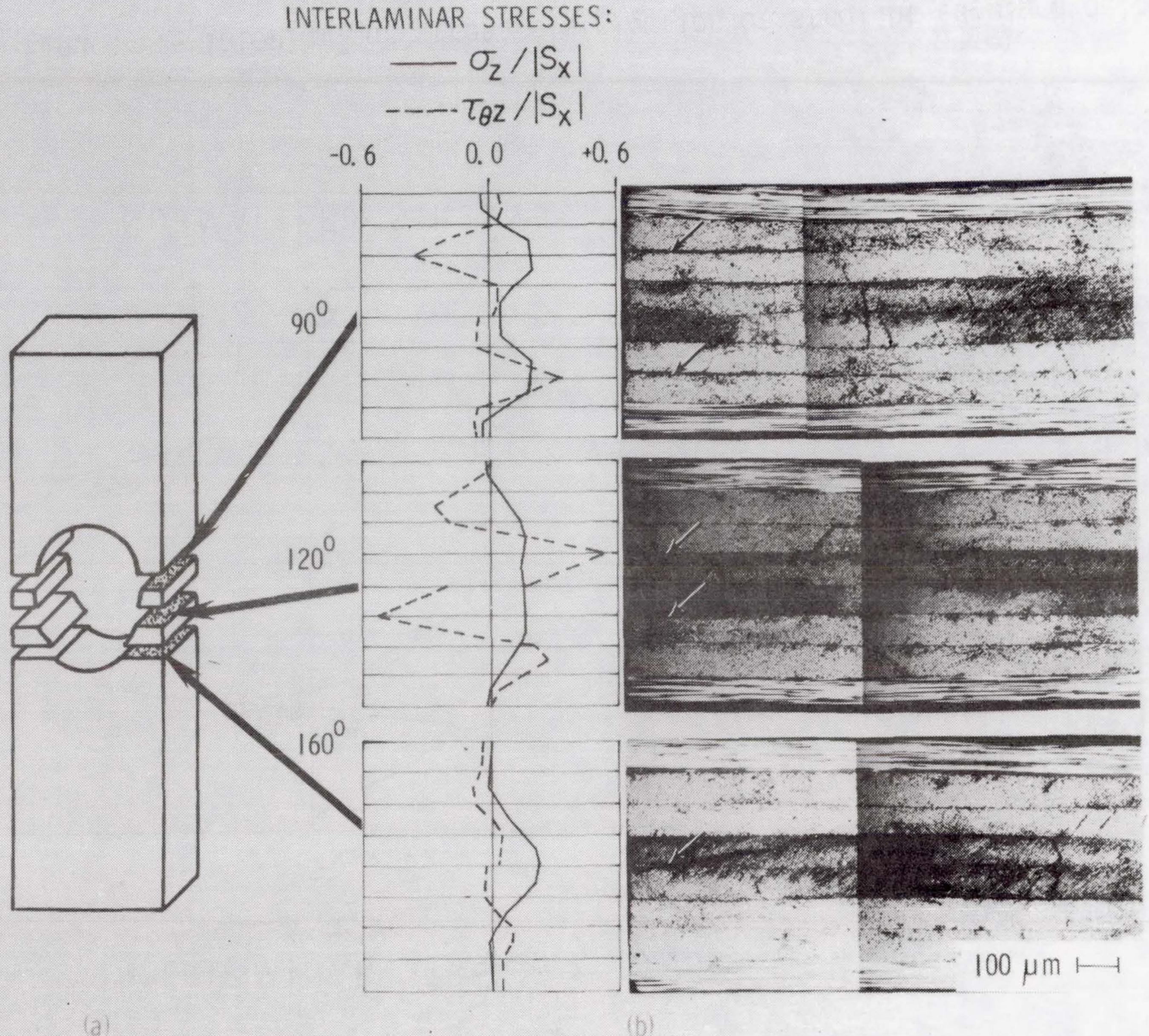

Figure 10.- Interlaminar stress distribution at edge of hole and delamination location for $(90/\pm45/0)_S$ specimen subjected to compression fatigue.

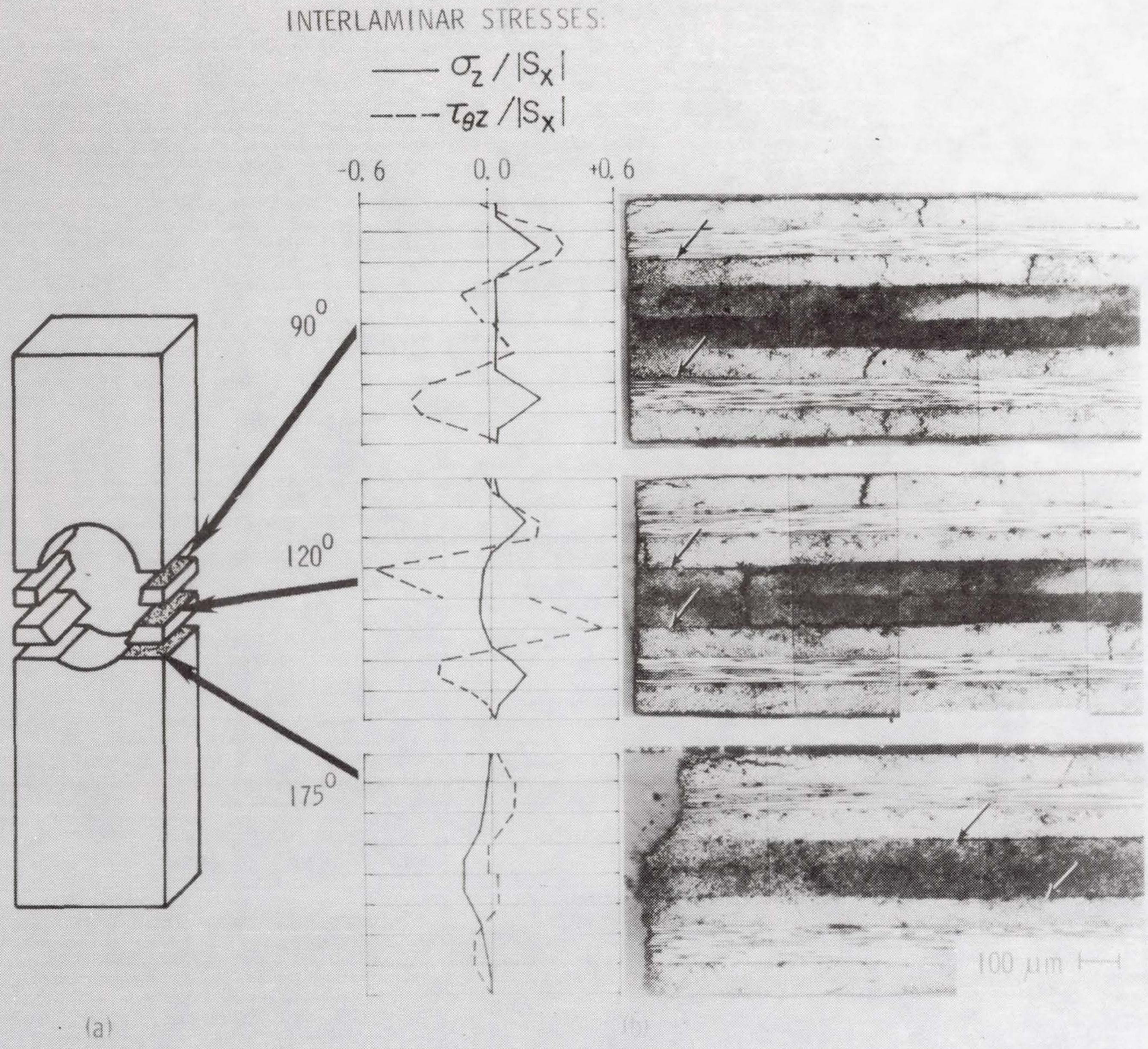

Figure 11.- Interlaminar stress distribution at edge of hole and delamination location for $(45/90/-45/0)_s$ specimen subjected to tension fatigue.

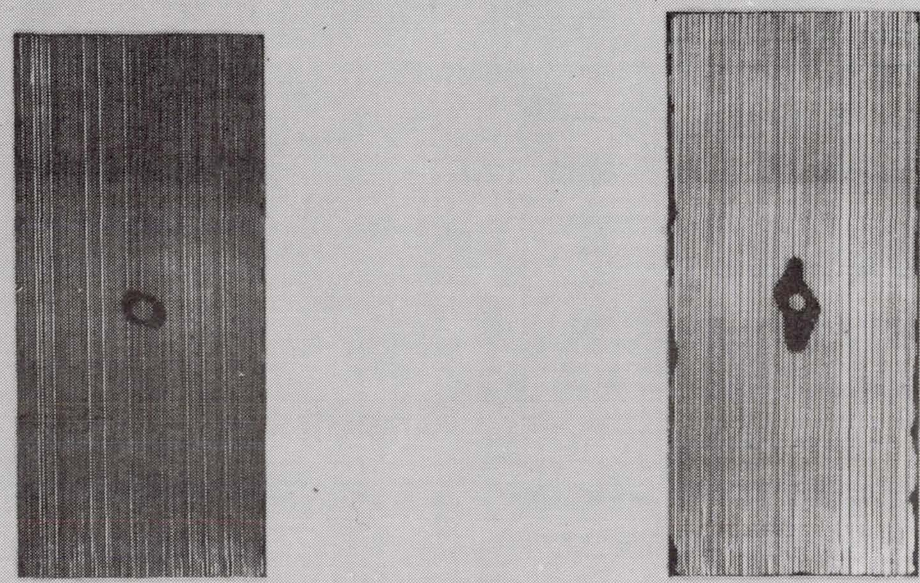

C-SCAN AFTER 6 x 10^6 CYCLES

C-SCAN AFTER 9 x 10^6 CYCLES

Figure 12.- Delamination zones at two points in fatigue life of $(90/\pm45/0)_s$ laminate $(S_{max}/S_{ult} = 80\%)$.

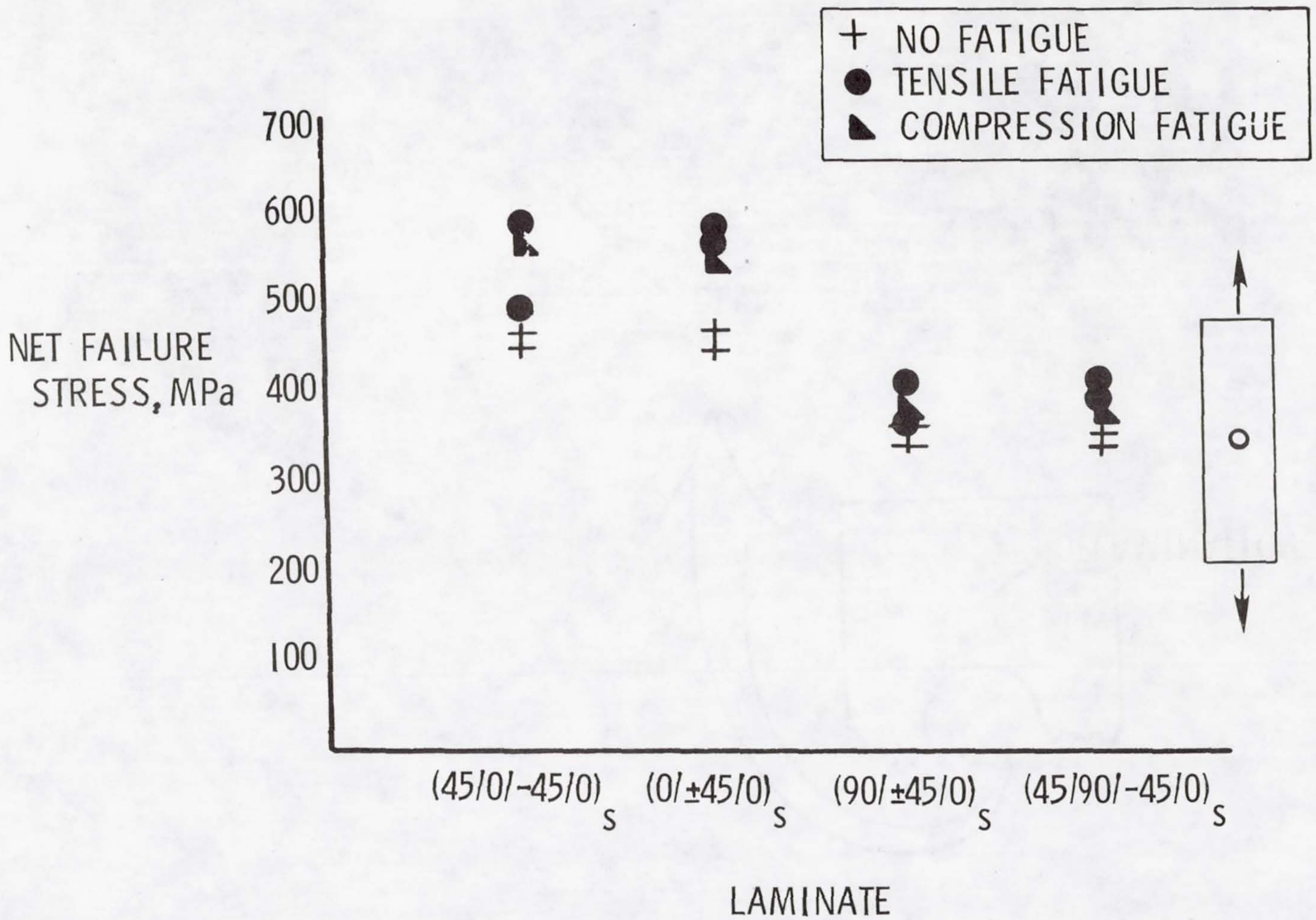

Figure 13.- Tensile strength of notched laminates after 10^7 cycles ($|S|_{max}/S_{ult}$ = 67%).

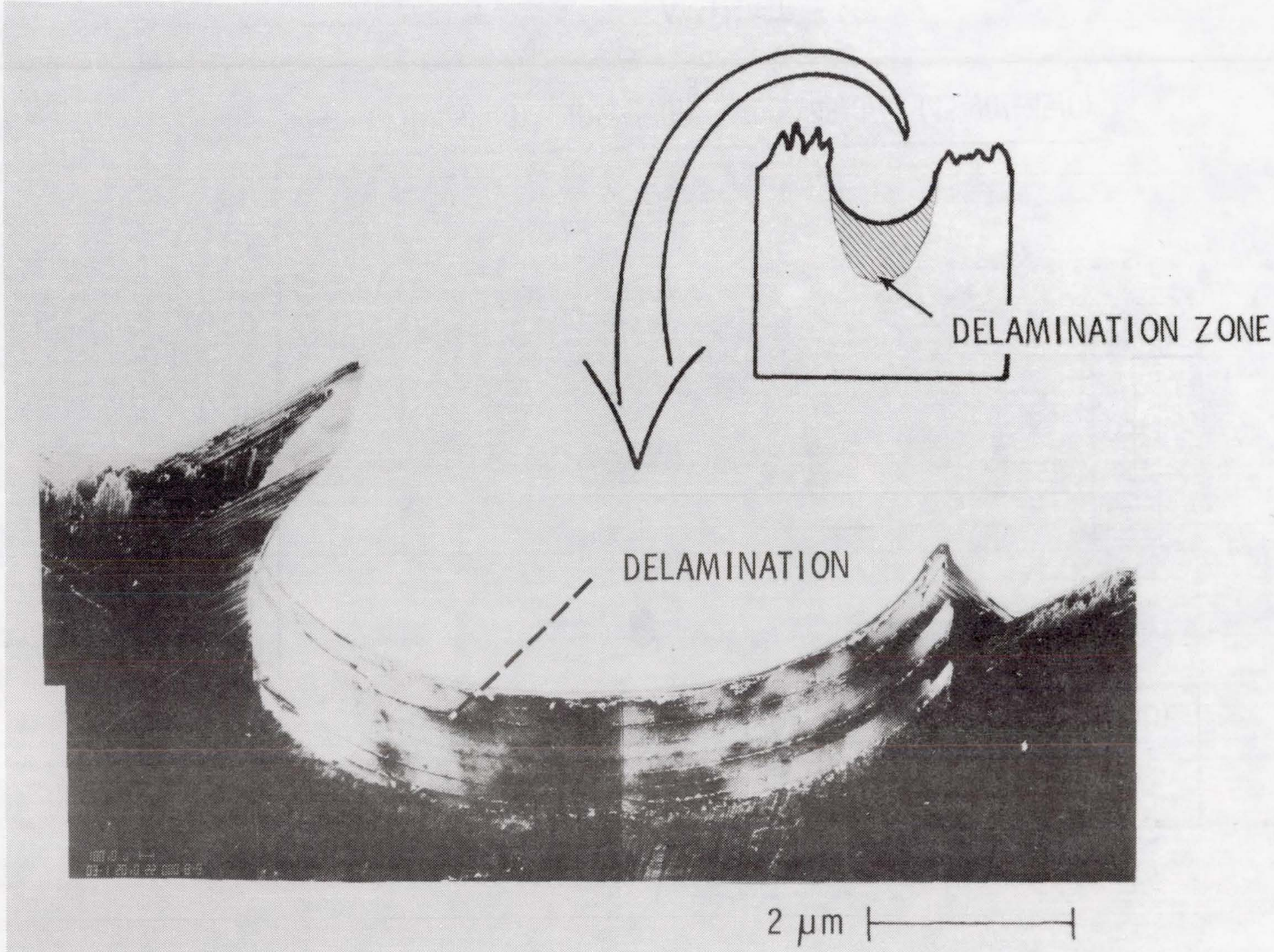

Figure 14.- SEM photograph of fractured $(0/\pm45/0)_S$ tensile fatigue specimen.

1. Report No.	2. Government Accession No.	3. Recipient's Catalog No.
NASA TM-80121		
4. Title and Subtitle EXPERIMENTAL AND ANALYTICAL STUDY OF FATIGUE DAMAGE IN NOTCHED GRAPHITE/EPOXY LAMINATES		5. Report Date June 1979 6. Performing Organization Code
7. Author(s) John D. Whitcomb		8. Performing Organization Report No.
9. Performing Organization Name and Address NASA Langley Research Center Hampton, VA 23665		10. Work Unit No. 506-17-23-03 11. Contract or Grant No.
12. Sponsoring Agency Name and Address National Aeronautics and Space Administration Washington, DC 20546		13. Type of Report and Period Covered Technical Memorandum 14. Sponsoring Agency Code

15. Supplementary Notes

Presented at the ASTM Symposium on the Fatigue of Fibrous Composite Materials, San Francisco, California, May 22-23, 1979.

16. Abstract

Fatigue damage development in notched $(0/\pm45/0)_s$, $(45/0/-45/0)_s$, $(90/\pm45/0)_s$, and $(45/90/-45/0)_s$ graphite/epoxy laminates was investigated. Both tension and compression fatigue behaviors were studied. Most of the tests were conducted at load levels equal to two-thirds of the ultimate tensile strength of the notched specimens. After fatigue loading, specimens were examined for damage type and location using visual inspection, light microscopy, scanning electron microscopy, ultrasonic C-scans, and X-radiography. Delamination and ply cracking were found to be the dominant types of fatigue damage. In general, ply cracks did not propagate into adjacent plies of differing fiber orientation. To help understand the varied fatigue observations, the interlaminar stress distribution was calculated with finite element analysis for the regions around the hole and along the straight free edge. Comparison of observed delamination locations with the calculated stresses indicated that both interlaminar shear and peel stresses must be considered when predicting delamination. The effects of the fatigue cycling on residual strength and stiffness were measured for some specimens of each laminate type. Fatigue loading generally caused only small stiffness losses. In all cases, residual strengths were greater than or equal to the virgin strengths.

17. Key Words (Suggested by Author(s))		18. Distribution Statement
Composite materials	Laminates	Unclassified - Unlimited
Failure mechanisms	Fatigue damage	
Stress analysis	Radiography	
Stress distribution	Microscopy	Subject Category 24

19. Security Classif. (of this report)	20. Security Classif. (of this page)	21. No. of Pages	22. Price*
Unclassified	Unclassified	30	$4.50

* For sale by the National Technical Information Service, Springfield, Virginia 22161